

# Hot-electron resonant terahertz bolometric detection in the graphene/black-AsP field-effect transistors with a floating gate

V. Ryzhii<sup>1</sup>, C. Tang<sup>1</sup>, T. Otsuji<sup>1</sup>, M. Ryzhii<sup>2</sup>, V. Mitin<sup>3</sup>, and M. S. Shur<sup>4</sup>

<sup>1</sup>Research Institute of Electrical Communication, Tohoku University, Sendai 980-8577, Japan

<sup>2</sup>Department of Computer Science and Engineering,  
University of Aizu, Aizu-Wakamatsu 965-8580, Japan

<sup>3</sup>Department of Electrical Engineering, University at Buffalo, SUNY, Buffalo, New York 14260 USA

<sup>4</sup>Department of Electrical, Computer, and Systems Engineering,  
Rensselaer Polytechnic Institute, Troy, New York 12180, USA

We evaluate the terahertz (THz) detectors based on field effect transistor (FET) with the graphene channel GC and a floating metal gate (MG) separated from the GC by a black-phosphorus (b-P) or black-arsenic (b-As) barrier layer (BL). The operation of these GC-FETs is associated with the heating of the two-dimensional electron gas in the GC by impinging THz radiation leading to thermionic emission of the hot electrons from the GC to the MG. This results in the variation of the floating gate potential, which affects the source-drain current. At the THz radiation frequencies close to the plasmonic resonance frequencies in the gated GC, the variation of the source-drain current and, hence, the detector responsivity can be resonantly large.

## I. INTRODUCTION

The specific properties of graphene channel (GCs) [1–3] and black-P (b-P), black-As (b-As), or black-AsP (b-AsP) layers [4–8] open up prospects for devices based on the GCs (see, for example, the review [9]) and on the GC/b-AsP heterostructures [6], including the electron devices using the real-space transfer over the b-AsP layers [10, 11] and different optoelectronic devices [12–15]. Due to relatively low energy barriers for the electrons and holes at the GC/b-AsP interface, the thermionic emission through such an interface can be effective, particularly, enabling the creation of the GC/b-AsP-bolometric terahertz (THz) detectors.

In this paper, we evaluate the characteristics of the bolometric detectors based on the field-effect transistor (FET) structures with the GC, b-AsP barrier layer (BL), and floating metal gate (MG). Similar GC/b-AsP FET detectors were recently proposed and analyzed by us [16]. The principal difference between the GC/b-AsP FETs considered previously and the GC/b-AsP FETs under consideration here is the floating MG. The idea of using MG in graphene bolometers has been applied to pyroelectric graphene mid-infrared detectors. In these detectors, pyroelectric substrate charge is collected by a floating gate [17].

In contrast, the operation of the bolometric detectors considered in this paper is associated with the thermionic emission of the electrons heated by the impinging THz radiation from the GC into the MG via the b-AsP BL. However, contrary to the devices studied in [16], in which the gate current serves as the detected signal, in the detector with the floating MG considered here the detected signal is associated with the variations of the source-drain current in the GC stimulated by the varying potential of the MG. The potential of the latter is controlled by the thermionic emission from the GC, which reinforces with

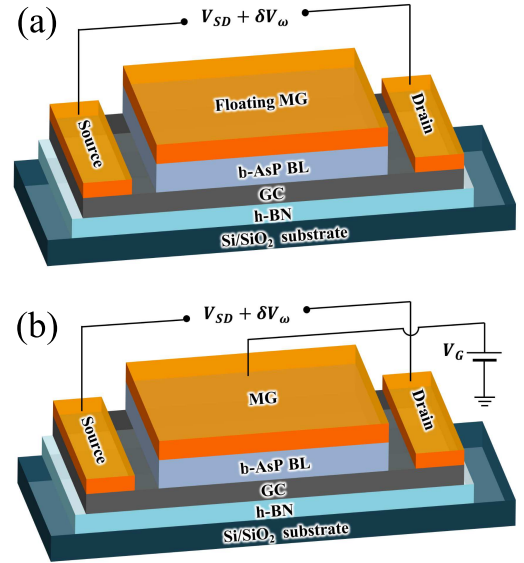


FIG. 1. Schematic view of the GC/b-AsP FET detectors (a) with the floating MG and (b) with the MG biased by the gate voltage  $V_G$  [16].

increasing THz power. This effect can become rather strong at the plasmonic oscillations resonantly excited by the impinging THz radiation in the gated GC [18–22]. The features of the GC-FET detector operation with the floating gate require the development of a fairly different device model. Using this model, we calculate the signal current and the detector responsivity as functions of the structural parameters. As demonstrated, the floating gate GC/b-AsP FET detectors might exhibit elevated values of the responsivity, particularly, at the plasmonic resonances. We also compare the performance of GC/b-AsP FET detectors with the floating and biased MGs.

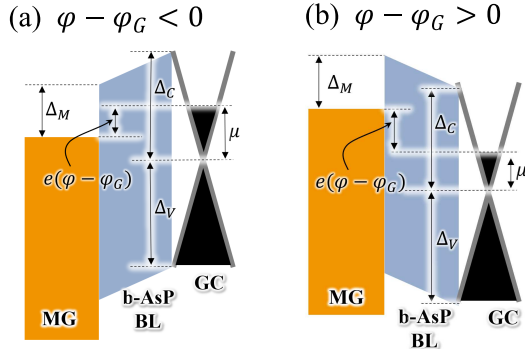


FIG. 2. Band diagrams of GC/b-AsP FET detector with the floating MG [shown in Fig. 1(a)] near (a) the source ( $x \gtrsim -L$ , the GC potential  $\varphi - \varphi_G < 0$ ) and (b) the drain ( $x \lesssim L$ , the GC potential  $\varphi - \varphi_G > 0$ ).

## II. ELECTRON TRANSPORT

We consider the GC/b-AsP FETs with the floating MG and the b-AsP gate BL. Figures 1 and 2 schematically show the cross-section of the device structures and their band diagrams. The bias voltage  $V_{SD}$  and the signal voltage  $\delta V_\omega$  are applied between the FET source and drain as shown in Fig. 1(a). The signal voltage is produced by an antenna receiving the impinging THz radiation with the frequency  $\omega$ . The GC of the FETs is doped by donors. For definiteness, the work functions of the gate metal and the b-AsP BL, and the GC doping level (the electron Fermi energy  $\mu_D$  in the GC in equilibrium when no bias is applied) are chosen to provide the band alignment in the equilibrium. This corresponds to  $\Delta_M = \Delta_C - \mu_D$ , where  $\Delta_M$  and  $\Delta_C$  are the differences between the work functions of the gate metal and the b-AsP BL and between the b-AsP BL and the GC.

At the source-drain bias voltage  $V_{SD}$  and the THz irradiation, the source-drain current,  $J_{SD}$ , and the electron effective temperature,  $T$ , in the GC averaged over the THz radiation period  $2\pi/\omega$  can be presented as

$$J_{SD} = \bar{J}_{SD} + \langle \delta J_\omega \rangle, \quad T = \bar{T} + \langle \delta T_\omega \rangle. \quad (1)$$

Here  $\bar{J}_{SD} = J_0 + \Delta \bar{J}_{DC}$  and  $\bar{T} = T_0 + \Delta \bar{T}$ ,  $J_0$  is the source-drain current at the 2DEG effective temperature equal to the lattice  $T_0$ ,  $\Delta \bar{J}_{DC}$  and  $\Delta \bar{T}$  are the pertinent current and temperature variations, and  $\langle \delta J_{SD} \rangle$  and  $\langle \delta T_\omega \rangle$  are the variations caused by the source-drain bias voltage  $V_{SD}$  and the signal voltage  $\delta V_\omega$ .

The source-drain current  $J_{SD}$  per unit of the GC width is governed by the following equations:

$$\frac{dJ_{SD}}{dx} = -j, \quad J_{SD} = -\sigma \frac{d\varphi}{dx}, \quad (2)$$

where  $j$  is the density of the thermionic current between the GC and the MG,  $\sigma = \sigma_D(\mu/\mu_D)$  and  $\sigma_D =$

$(e^2 \mu_D / \pi \hbar^2 \nu)$  is the electron Drude conductivity in equilibrium with  $\nu$  being the characteristic electron scattering frequency in the GC (the inverse electron momentum relaxation time), and  $\mu$  is the electron Fermi energy, which generally differs from  $\mu_D$  due to the MG charging.

The averaged GC potential  $\varphi$  (dependent on the coordinate  $x$  directed along the GC) satisfies the following conditions at the source and drain contacts:

$$\varphi|_{x=\pm L} = \pm \frac{V_{SD}}{2}, \quad (3)$$

where  $2L$  is the spacing between the contacts (the GC length). Considering the difference between the GC potential  $\varphi$  and the MG potential  $\varphi_G$  and accounting for the quantum capacitance [23, 24] of the gated GC, at not too-large potential swing ( $\varphi - \varphi_G$ ) we obtain

$$\mu \simeq \mu_D - \varkappa e(\varphi - \varphi_G). \quad (4)$$

Here  $\varkappa = \mu_0 / (\mu_0 + \mu_D)$ ,  $\mu_0 = \kappa \hbar^2 v_W^2 / 8e^2 W$ ,  $\kappa$  is the BL dielectric constant, and  $v_W \simeq 10^8$  cm/s is the electron velocity in GCs. This implies that an increase in  $\varphi$  leads to an increase in the 2DEG density and, hence, its Fermi energy  $\mu$ . The contribution of the quantum capacitance to Eq. (4) is characterized by a factor  $\mu_0 / \mu_D \propto W^{-1}$ .

Since the MG is disconnected (floating MG),

$$\int_{-L}^L dx j = 0. \quad (5)$$

Due to the trapezoid shape of the barrier between the GC and the MG, the potential barrier heights for the electron emitted from the GC and the MG,  $\Delta_{BL}^{\leftarrow}$  and  $\Delta_{BL}^{\rightarrow}$ , are equal to:

$\Delta_{BL}^{\leftarrow} = \Delta_M + e(\varphi - \varphi_G)$  and  $\Delta_{BL}^{\rightarrow} = \Delta_M$  for  $\varphi > \varphi_G$ , and

$\Delta_{BL}^{\leftarrow} = \Delta_M - (\mu - \mu_D)$  and  $\Delta_{BL}^{\rightarrow} = \Delta_M - (\mu - \mu_D) - e(\varphi - \varphi_G)$  for  $\varphi < \varphi_G$ .

In this situation, the density of the thermionic current,  $j$ , between the GC and the MG is given by

$$j = j^m \left[ \exp\left(-\frac{\Delta_M + e(\varphi - \varphi_G)}{T}\right) - \exp\left(-\frac{\Delta_M}{T_0}\right) \right] \quad (6)$$

when  $\varphi - \varphi_G > 0$ , and

$$j = j^m \left[ \exp\left(-\frac{\Delta_M - (\mu - \mu_D)}{T}\right) - \exp\left(-\frac{\Delta_M - (\mu - \mu_D) - e(\varphi - \varphi_G)}{T_0}\right) \right] \quad (7)$$

when  $\varphi - \varphi_G < 0$ . Here  $j^m \simeq e\Sigma/\tau_\perp$  is the maximum current density,  $\Sigma$  is the electron density in the G-channel,

and  $\tau_{\perp}$  is the characteristic try-to-escape time from the G-channel. From Eqs. (2), (4), (6), and (7), we obtain

$$= \eta \left[ \exp\left(\frac{\Delta_M(T-T_0)}{T_0 T}\right) \exp\left(-\frac{e(\varphi-\varphi_G)}{T}\right) - 1 \right] \quad (8)$$

when  $\varphi - \varphi_G > 0$ , and

$$= \eta \left[ \exp\left(\frac{\Delta_M(T-T_0)}{T_0 T}\right) \exp\left(-\frac{e(\varphi-\varphi_G)}{T}\right) - \exp\left((1-\kappa)\frac{e(\varphi-\varphi_G)}{T_0}\right) \right] \quad (9)$$

when  $\varphi - \varphi_G < 0$ .

Here

$$\eta = \frac{e j^m}{\mu_D \sigma_D} \exp\left(-\frac{\Delta_M}{T_0}\right) = \frac{\nu L^2}{\tau_{\perp} v_W^2} \exp\left(-\frac{\Delta_M}{T_0}\right). \quad (10)$$

Setting, for example,  $\Delta_M = 85$  meV,  $T_0 = 25$  meV,  $\nu = 1$  ps<sup>-1</sup>,  $\tau_{\perp} = 10$  ps,  $L = 1.0$   $\mu$ m,  $\kappa = 4 - 6$ ,  $W = 10$  nm, and  $\mu_D = 140$  meV, we obtain  $\eta \simeq (3.3) \times 10^{-3}$  and  $\kappa \simeq 0.088 - 0.127$  [ $\mu_0 \simeq (13.6 - 20.4)$  meV].

At low or moderate bias source-drain voltages and THz radiation powers,  $\psi$  and  $|T - T_0|/T_0$  are small. In this case, linearizing Eqs. (8) and (9), we arrive at

$$L^2 \frac{d^2}{dx^2} \left[ e(\varphi - \varphi_G) + \frac{\kappa e^2 (\varphi - \varphi_G)^2}{2 \mu_D} \right] \simeq \frac{\eta \mu_D}{T_0} \left[ \frac{\Delta_M}{T_0} (T - T_0) - e(\varphi - \varphi_G) \right] \quad (11)$$

Equation (11) corresponds to the thermionic current density

$$j \simeq \frac{j^m}{T_0} \left[ \frac{\Delta_M}{T_0} (T - T_0) - e(\varphi - \varphi_G) \right]. \quad (12)$$

Using Eq. (11) with Eq. (3) and taking into account the smallness of parameter  $\eta$  [i.e., neglecting the term in the right-hand side of Eq. (11)], for the source-drain current  $J_{SD} = \sigma(HV_{SD}/2L) = \sigma_D(\mu/\mu_D)(HV_{SD}/2L)$  with the pertinent accuracy we obtain

$$J_{SD} \simeq \sigma_D \left( 1 + \kappa \frac{e\varphi_G}{\mu_D} \right) \frac{H}{2L} V_{SD}. \quad (13)$$

Using Eqs. (5) and (12), we find the MG potential:

$$e\varphi_G = \frac{eV_{SD}}{4} - \frac{\Delta_M}{2L} \int_{-L}^L dx \frac{(T - T_0)}{T_0}. \quad (14)$$

The latter equation corresponds to an increase in the source-drain current with increasing gate potential  $\varphi_G$  (due to an increase in the Fermi energy and, hence, the G-channel conductivity). One can see that an increase in the 2DEG effective temperature leads to the intensification of the electron transfer from the G-channel to the gate which results in its lower potential.

Equations (13) and (14) for the source-drain current components yield

$$\bar{J}_{SD} \simeq J_0 \left[ 1 + \frac{\kappa}{\mu_D} \left( eV_{SD} - \frac{\Delta_M}{2L} \int_{-L}^L dx \frac{(\bar{T} - T_0)}{T_0} \right) \right] \quad (15)$$

and

$$\langle \delta J_{\omega} \rangle \simeq -J_0 \frac{\kappa \Delta_M}{\mu_D} \frac{\langle \langle \delta T_{\omega} \rangle \rangle}{T_0} \quad (16)$$

with  $J_0 = \sigma_D V_{SD} (H/2L)$  and  $\langle \langle \delta T_{\omega} \rangle \rangle = \int_{-L}^L dx \langle \delta T_{\omega} \rangle / 2L$  and  $H$  being the effective temperature average of the THz period and the GC length and the GC width, respectively. The quantity  $\langle \delta J_{\omega} \rangle$  given by Eq. (16) represents the response of the GC-FET to the impinging THz radiation.

### III. ELECTRON HEATING AND HEAT TRANSPORT

The electron heat transport equation can be presented as

$$-h \frac{d^2 T}{dx^2} + \frac{T - T_0}{\tau_{\varepsilon}} + \frac{\Delta_C \Delta_M}{\tau_{\perp} T_0} \exp\left(-\frac{\Delta_M}{T_0}\right) \left[ \frac{\Delta_M}{T_0} (T - T_0) - e(\varphi - \varphi_G) \right] \simeq \frac{\sigma}{\Sigma} \left[ \left( \frac{V_{SD}}{2L} \right)^2 + \frac{\text{Re} \sigma_{\omega}}{\sigma} \langle |\delta E_{\omega}|^2 \rangle \right] \quad (17)$$

For the variation of the 2DEG averaged effective temperature  $\langle \delta T_{\omega} \rangle$ , in view of Eqs. (5) and (12), Eq. (17) yields

$$-h \frac{d^2 \langle \delta T_{\omega} \rangle}{dx^2} + \frac{\langle \delta T_{\omega} \rangle}{\tau_{\varepsilon}} + \frac{\Delta_C \Delta_M}{\tau_{\perp} T_0} \exp\left(-\frac{\Delta_M}{T_0}\right) \left( \frac{\langle \delta T_{\omega} \rangle - \langle \langle \delta T_{\omega} \rangle \rangle}{T_0} \right) \simeq \frac{\text{Re} \sigma_{\omega}}{\Sigma} \langle |\delta E_{\omega}|^2 \rangle. \quad (18)$$

Here  $h \simeq v_W^2 / 2\nu$  is the electron thermal conductivity (per electron),  $\tau_{\varepsilon}$  is the electron energy relaxation time,  $\text{Re} \sigma_{\omega} = \sigma_D \nu^2 / (\nu^2 + \omega^2)$  is the real part of the 2DEG ac conductivity, and  $\delta E_{\omega}$  is the signal electric fields in the G-channel created due to the THz signals. The first, second,

TABLE I. Parameters of the GC/b-As and GC/b-P FET detectors and their responsivities.

Structure	$\Delta_M$ (meV)	$\Delta_C$ (meV)	$\mu_D$ (meV)	$L$ ( $\mu\text{m}$ )	$\Omega/2\pi$ (THz)	$\nu$ ( $\text{ps}^{-1}$ )	$\theta$	$\mathcal{L}$ ( $\mu\text{m}$ )	$R_\Omega^V$ (V/W)
GC/b-P/Al	85	225	140	1.0	1.136	1.0 - 2.5	1.02	1.58 - 1.00	$(2.1 - 1.8) \times 10^3$
GC/b-As/Ti	70	190	120	1.0	1.052	1.0 - 2.5	1.29	0.93 - 0.59	$(2.7 - 2.3) \times 10^3$

and third terms in the left-hand side of Eq. (18) are associated with the removal of the electron heat through the contact (due to a substantial electron lateral heat conductivity along the GC [25, 26]), the transfer to the lattice (primarily due to the interaction with optical phonons in the GC and the interface optical phonons [27–31]) and the MG over the BL (i.e., corresponding to the Peltier cooling [32, 33]), respectively. The term on the right-hand side of Eq. (13) corresponds to the 2DEG Joule heating.

We use the following boundary conditions for Eq. (18):

$$\langle \delta T_\omega \rangle|_{x=\pm L} = 0. \quad (19)$$

For the THz radiation asymmetric input via the antenna corresponding to the signal potential at the contacts equal to  $\pm \delta V_\omega/2$ , accounting for the excitation of plasmonic oscillations in the GC we obtain

$$\langle |\delta E_\omega|^2 \rangle = \frac{1}{2} \left( \frac{\delta V_\omega}{2L} \right)^2 \left| \frac{\gamma_\omega \cos(\gamma_\omega x/L)}{\sin \gamma_\omega} \right|^2. \quad (20)$$

Here  $\gamma_\omega = \pi \sqrt{\omega(\omega + i\nu)}/\Omega$  and  $\Omega = (2\pi e/\hbar L) \sqrt{\mu W/\kappa}$  are the effective wavenumber and the plasmonic frequency, respectively, with  $\kappa$  and  $W$  being the dielectric constant of the BL and its thickness,

Restricting our consideration by the most interesting case of the pronounced fundamental plasmonic resonance in the G-channel ( $\omega = \Omega \gg \nu$ ) and using Eq (15), we obtain

$$\text{Re} \sigma_\Omega \langle |\delta E_\Omega|^2 \rangle \simeq 2\sigma_D \cos^2 \left( \frac{\pi x}{L} \right) \left( \frac{\delta V_\Omega}{2L} \right)^2. \quad (21)$$

One needs to note that the Joule power at the plasmonic resonance given by Eq. (21) exceeds that at low frequencies (at least near  $x \simeq 0$ ) by a factor  $\sim (2\Omega/\pi\nu)^2$ .

Solving Eq. (18) accounting for boundary condition (19) and Eq. (21), for the values  $\langle \langle \delta T_\omega \rangle \rangle$  at the fundamental plasmonic resonance we obtain

$$\langle \langle \delta T_\Omega \rangle \rangle \simeq \frac{2\pi\sigma_D \hbar^2 v_W^2}{\mu_D^2} \frac{\tau_\varepsilon \Theta}{(1+\theta)} \left( \frac{\delta V_\Omega}{2L} \right)^2. \quad (22)$$

Here

$$\Theta = \left[ \frac{1 - \frac{\mathcal{L}}{L} \tanh\left(\frac{L}{\mathcal{L}}\right)}{1 + \frac{\mathcal{L}}{L} \tanh\left(\frac{L}{\mathcal{L}}\right)} \right] \quad (23)$$

is the factor characterizing the role of electron thermal transport, and

$$\theta = \frac{\tau_\varepsilon}{\tau_\perp} \frac{\Delta_C \Delta_M}{T_0^2} \exp\left(-\frac{\Delta_M}{T_0}\right), \quad \mathcal{L} = \sqrt{\frac{\hbar \tau_\varepsilon}{(1+\theta)}},$$

The characteristic length  $\mathcal{L}$  is the electron heat transfer (cooling) length.

Equations (16) and (22) yield

$$-\langle \delta J_\Omega \rangle \simeq \frac{2\pi\sigma_D^2 \hbar^2 v_W^2}{\mu_D^2 T_0} \left( \frac{\varkappa \Delta_M}{\mu_D} \right) \frac{\tau_\varepsilon \Theta}{(1+\theta)} \left( \frac{H V_{SD}}{2L} \right) \left( \frac{\delta V_\Omega}{2L} \right)^2. \quad (24)$$

The sign "minus" in Eq. (24) reflects the fact that the THz irradiation leads to an increase in the electron effective temperature, reinforcement of the electron emission from the GC and, hence, to a negative charging of the MG. The latter, in turn, decreases the source-drain current in the donor-doped GC.

#### IV. DETECTOR RESPONSIVITY

Considering that for the half-wavelength dipole antenna with the gain  $g$  one obtains  $\delta V_\Omega^2 = 32P_\Omega/gc$ , where  $P_\Omega$  is the THz power at the frequency  $\omega = \Omega$  collected by the detector antenna and  $c$  is the speed of light in vacuum, and accounting for that the GC channel resistance is equal to  $r_{SD} = 2L/H\sigma_D$ , for the detector voltage responsivity  $R_\Omega^V = |\langle \delta J_\Omega \rangle| r_{SD}/P_\Omega$  (at the radiation frequency corresponding to the fundamental plasmonic resonance), we obtain

$$\begin{aligned} R_\Omega^V &\simeq \frac{16e^2}{gc\mu_D^2} \left( \frac{L_\varepsilon}{L} \right)^2 \left( \frac{\varkappa \Delta_M}{T_0} \right) \Theta V_{SD} \\ &= \frac{16}{137g} \frac{\hbar}{\mu_D^2} \left( \frac{L_\varepsilon}{L} \right)^2 \left( \frac{\varkappa \Delta_M}{T_0} \right) \Theta V_{SD}. \end{aligned} \quad (25)$$

Here  $L_\varepsilon = \sqrt{\frac{v_W^2 \tau_\varepsilon}{\nu(1+\theta)}}$ .

The quantities  $\Delta_M$ ,  $\mu_D$ , and  $\varkappa$ , are determined by the material of the MG and the molar fractions of As in the BL (due to the condition  $\Delta_M = \Delta_C - \mu_D$  assumed in our model).

Examples of the parameters of the GC-FET detectors based on Al/b-P/GC and Ti/b-As/GC heterostructures (see, for example, Refs. [34] and [35]) and the estimates of their resonant responsivity are listed in Table I. We

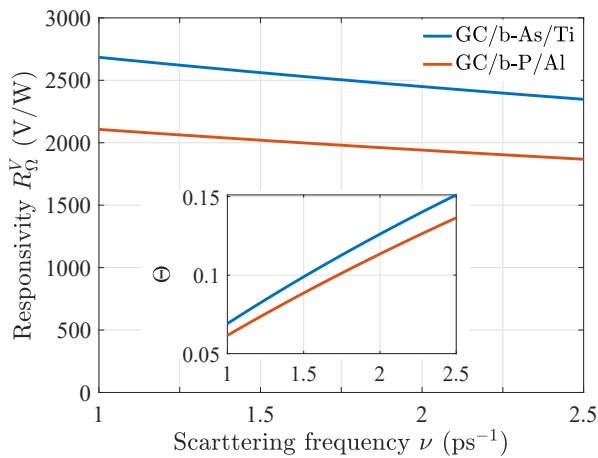


FIG. 3. Resonant responsivity  $R_{\Omega}$  of the GC/b-As/Ti (blue line) and GC/b-P/Al (red line) FET detectors and electron thermal transport factor  $\Theta$  (inset) as functions of electron scattering frequency  $\nu$ .

assume also that  $\kappa = 4$ ,  $\tau_{\varepsilon} = 10$  ps,  $\tau_{\perp} = 10$  ps,  $W = 10$  nm,  $T_0 = 25$  meV ( $\sim 300$  K), and  $V_{SD} = 1.6$  V. The above parameters (with  $\nu = 1$  ps $^{-1}$  and  $H = 2L$  or with  $\nu = 2.5$  ps $^{-1}$  and  $H = 5L$ ) correspond to the GC-FET detector resistances  $r_{SD} \simeq 55$   $\Omega$  and  $r_{SD} \simeq 64$   $\Omega$ , respectively (at  $H = 2L$ ). One needs to note that at the above parameters the electron thermal transport factor depending on the ratio  $\mathcal{L}/L$  in Eq. (23) is rather small (about 0.061 – 0.151 at  $\nu = 1$  ps $^{-1}$ ) substantially decreasing the responsivity. The role of the electron cooling due to the thermal transport to the side contacts can be decreased by increasing  $\nu$  (this decreases the electron thermal conductivity) or choosing the longer GC length  $L$ .

Figure 3 shows the responsivity of the GC/b-AsP and GC/b-As FETs with a floating MG at  $\omega = \Omega$  (i.e., at the fundamental plasmonic resonance) calculated for the main parameters corresponding to Table I but for different electron scattering frequencies  $\nu$ . For the definiteness, we set  $V_{SD} = 1.6$  V. The inset in Fig. 3 shows how the role of the electron thermal transport along the GC changes with varying scattering frequencies. The pertinent dependence is associated with the  $h$  vs  $\nu$  dependence. As follows from Fig. 3, an increase in  $\Theta$  (i.e., a weakening of the electron heat transfer to the source and drain contacts when  $\nu$  becomes larger) leads to slowing of the  $R_{\Omega}^V$  vs  $\nu$  dependence. Thus, a relatively weak dependence of  $R_{\Omega}^V$  on  $\nu$  is interpreted by the decrease in the electron system Joule heating in the GC by the signal electric field (because of  $\sigma_D \propto \nu^{-1}$ ) accompanied with a decrease in the power transferred to the source and drain contacts.

Figure 4 shows the spectral dependences of the responsivity,  $R_{\omega}^V$ , of the GC/b-As and GC/b-P detectors calculated for different  $\nu$  and the same parameters as for Fig. 3. We limited our consideration by the signal frequencies around the fundamental plasmonic resonance, where the obtained dependences exhibit pronounced maxima pro-

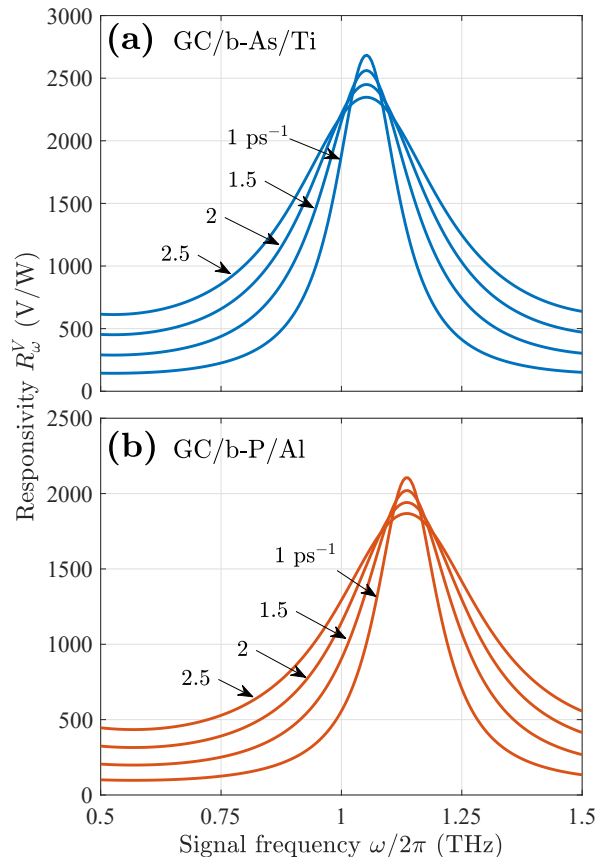


FIG. 4. Responsivity  $R_{\omega}$  of the (a) GC/b-As/Ti and (b) GC/b-P/Al FET detectors vs signal frequency  $\omega/2\pi$  for different values of electron scattering frequency  $\nu$ .

vided that  $\Omega \gg \nu$ . As seen from Fig. 4, an increase in  $\nu$  gives rise to a smearing of the resonant peak. In a wider frequency range, the responsivity of the detectors under consideration is a profoundly oscillatory function of the radiation signal frequency  $\omega$  with a set of the maxima at the plasmonic resonances  $\omega = n\Omega$  ( $n$  is the resonance index). These oscillations are described by the relation, which follows from the above equations:

$$R_{\omega}^V \propto \text{Re}\sigma_{\omega} \left| \frac{\gamma_{\omega} \cos(\gamma_{\omega} x/L)}{\sin \gamma_{\omega}} \right|^2. \quad (26)$$

As follows from Eq. (26), the dependences  $R_{\omega}^V$  vs  $\omega/2\pi$  exhibit the alternation of sharp maxima and relatively deep minima. At the intermediate frequencies, the responsivity at the minima, is smaller than the resonant responsivity by a factor of  $(\pi\nu/2\Omega)^2 \ll 1$ . At elevated collision frequencies  $\nu$ , the spectral characteristics of  $R_{\omega}^V$  become smoother. However, up to  $(\pi\nu/2\Omega)^2 \sim 1$  (this corresponds to  $\nu \sim 4$  ps $^{-1}$ , at the plasmonic resonances and between the resonances the responsivity can be still relatively high. Hence, the non-resonant response can also be useful.

## V. COMMENTS

Above we assumed that  $J_{SD} \propto \sigma \propto \mu$ . Theoretical studies show that the doped GC ( $\mu_D \gg T_0$ ) conductivity  $\sigma$  can exhibit different dependences on  $\mu$  [36–38]. In particular, it can vary from  $\sigma$  virtually independent of  $\mu$  if the short-range scattering of electrons is dominant to  $\sigma \propto \mu^2$  in the case of the long-range scattering (for example, on charged clusters) [38]. In the first situation  $\nu \propto p$ , where  $p$  is the electron momentum. In the second case,  $\nu \propto p^{-1}$ . In this regard, our model corresponds to an intermediate  $\sigma$  vs  $\mu$  relation (see, for example, Ref. 37), in which the momentum dependence of  $\nu$  is disregarded. This provides  $\sigma \propto \sqrt{\Sigma} \propto \sqrt{V_G}$  ( $V_G$  is the voltage swing between the GC and the gate). The latter qualitatively agrees with the experimental data [1]. In such a case, setting  $\nu = \text{constant}$  (see, for example, Ref. 38), we obtain the relation

$$\begin{aligned} \sigma &= \frac{e^2 T}{\pi \hbar^2 \nu} \int_0^\infty d\xi \xi \frac{d}{d\xi} \left[ -\frac{1}{\exp(\xi - \mu/T) + 1} \right] \\ &= \frac{e^2}{\pi \hbar^2 \nu} [\mu + T \ln(1 + e^{-\mu/T})] \simeq \frac{e^2 \mu}{\pi \hbar^2 \nu}, \end{aligned} \quad (27)$$

which was used above.

Considering that the resonant voltage responsivity,  $R_\omega^{V,GG}$ , of GC/b-AsP FETs with the biased gate can be estimated as [16]

$$R_\omega^{V,GG} \sim \frac{16\pi^2}{137} \frac{\hbar}{eT_0} \frac{\tau_\varepsilon}{\tau_\perp} \frac{\Delta_M}{T_0} \exp\left(-\frac{\Delta_M}{T_0}\right), \quad (28)$$

for the ratio of the voltage responsivities we obtain

$$\frac{R_\Omega^V}{R_\Omega^{V,GG}} \simeq \frac{\varkappa}{2} \left(\frac{L_\varepsilon}{L}\right)^2 \left(\frac{\tau_\varepsilon}{\tau_\perp}\right) \left(\frac{T_0}{\mu_D}\right) \exp\left(\frac{\Delta_M}{T_0}\right) \left(\frac{eV_{SD}}{\mu_D}\right) \quad (29)$$

For the typical parameters used above and  $V_{SD} \sim (10 - 25)$  mV, the latter ratio is about unity, although it increases with further (linearly) increase in  $V_{SD}$ . The latter might be limited by the lattice heat removal via the substrate and the contacts. Setting  $\nu = (1 - 2)$  ps<sup>-1</sup>, for the thermal power we obtain  $P_{Th} \sim (0.3 - 0.7)$  mW at  $V_{SD} = 0.2$  V and  $P_{Th} \sim (41 - 47)$  mW at  $V_{SD} = 1.6$  V.

As follows from the obtained results, both the current and voltage responsivities are proportional to the source-drain bias voltage  $V_{SD}$ . The dark current is also proportional to  $V_{SD}$ . This implies that the noise-equivalent power (NEP) and the dark current-limited detectivity of the detectors under consideration vary with increasing source-drain voltage as  $\text{NEP} \propto 1/\sqrt{V_{SD}}$  and  $D_\Omega^* \propto \sqrt{V_{SD}}$ , respectively.

For the GC/b-As and GC/b-P detectors with the above parameters at  $V_{SD} = 1.6$  V, we obtain  $\text{NEP} \simeq 2.2$  pW/Hz<sup>1/2</sup> and  $\text{NEP} \simeq 2.5$  pW/Hz<sup>1/2</sup> (for the GC/b-As and GC/b-P FETs, respectively), which appears to

be promising (compare with other THz bolometers [9]). If  $\sqrt{2LH} = 2$   $\mu\text{m}$ , the latter corresponds to  $D_\Omega^* \simeq 9 \times 10^7$  cm Hz<sup>1/2</sup>/W  $\simeq 8 \times 10^7$  cm Hz<sup>1/2</sup>/W, which is about of or exceeding the detectivity of other uncooled THz bolometers (see, for example, Ref. 39). However, one needs to note that NEP increases and  $D_\Omega^*$  decreases with increasing  $\nu$ .

Since the operation speed of the detectors under consideration is determined by the characteristic times of the electron cooling,  $t_\theta \lesssim \tau_\varepsilon/(1 + \theta)$ , associated with the energy relaxation on phonons and the heat transfer over the BL, and the gate recharging time. The latter is estimated as  $t_{rc} \sim \tau_\perp (2T_0\mu_0/\mu_D^2) \exp(\Delta_M/T_0)$ . The comparison of these characteristic times yields

$$\frac{t_\theta}{t_{rc}} \simeq \frac{\tau_\varepsilon}{\tau_\perp(1 + \theta)} \left(\frac{\mu_D^2}{2T_0\mu_0}\right) \exp\left(-\frac{\Delta_M}{T_0}\right). \quad (30)$$

For the device structural parameters assumed above  $T_0 = 25$ , we obtain  $t_\theta/t_{rc} \sim 0.5$ . This implies that the GC/b-AsP FET bolometers response time is about  $t_r \sim t_\theta + t_{rc} \sim 20$  ps.

The values of the collision frequencies used in the above calculations can be expressed via the electron mobility  $M$ . Using the relation  $M = ev_W^2/\mu_D\nu$ , where  $m = \mu/v_W^2$  is the so-called fictitious electron mass in GCs, for  $\mu_D = 140$  meV and  $\nu = (1 - 4)$  ps<sup>-1</sup>, we obtain the range  $M \simeq (1.78 - 7.14) \times 10^4$  cm/V·s (compare, for example, with Refs. 40, and 41). According to the estimates [41], the room temperature mobility in the GCs on h-BN at the electron density corresponding to the above the Fermi energy can be about  $m \simeq 10^5$  cm/V·s. The latter corresponds to  $\nu \simeq 0.714$  ps<sup>-1</sup>. The quality of the interface between the GC (placed atop of h-BN) and the b-P BL can limit the values of  $M$  and  $\nu$ . The pertinent room temperature electron mobility obtained experimentally several years ago is equal to  $M \simeq (7 - 8) \times 10^3$  cm/Vs [42] ( $M$  exceeds  $10^4$  cm/Vs at  $T_0 \leq 200$  K). This corresponds to not too small  $\nu$ . One can expect that the contemporary technology is able to provide the GC/b-P interface with sufficiently small  $\nu$ , at which the parameter  $((\pi\nu/2\Omega)^2 < 1)$ , so that the plasmonic resonances are pronounced. A substantial reinforcement of the plasmonic resonances in the GC-FET detectors can be realized in the case of the composite gate BL, which includes a relatively narrow b-P BL (and the MG) and the h-BN (or WSe<sub>2</sub> [43]) sections between the b-P section and the source in drain. In such a GC-FET detector, the sharpness of the plasmonic resonances might be determined by the GC main part (encapsulated by h-BN and providing small electron collision frequency), by the thermionic current flows via the narrow b-P window.

Similar THz detection properties can be expected in the GC/b-AsP FET devices with the floating isolated doped graphene gate (GG). The main distinction between the detectors with the MG and the detectors with the GG is the different plasmonic response in the latter

because of the GG influence on the plasmonic oscillations in the double-graphene structures [44–46]. Another option is to use the MG consisting of an array of metallic islands (MIs) or quantum dots (QDs). In such a case, each MI/QD has its own floating potential determined by the electron exchange between the MG/QD and the GC (compare with the devices analyzed in Ref. 9). Due to this, the potential distribution along the GC and the effect of the floating MG on the source-drain current can be markedly different from that considered above. However, the consideration of the detectors in question requires a proper modification of the device model and, therefore, a separate treatment.

## VI. CONCLUSIONS

We estimated the room temperature characteristics of the proposed GC/b-AsP FETs with the floating MG operating in the THz frequency range at room temperature. We showed that these detectors can exhibit high values of responsivity at the plasmonic resonances ( $\gtrsim 10^3$  V/W)

and rather short response times ( $\sim 20$  ps).

## AUTHOR CONTRIBUTIONS

All authors contributed equally to this work.

## ACKNOWLEDGMENTS

The Japan Society for Promotion of Science (KAKENHI Grants # 21H04546 and # 20K20349), Japan; RIEC Nation-Wide Collaborative Research Project # R04/A10; the US Office of Scientific, Research Contract N00001435, (Project Monitor Dr. Ken Goretta).

## CONFLICT OF INTEREST

The authors declare no conflict of interest

## DATA AVAILABILITY

All data that support the findings of this study are available within the article.

---

## REFERENCES

- [1] A. H. Castro Neto, F. Guinea, N. M. Peres, K. S. Novoselov, and A. K. Geim, “The electronic properties of graphene,” *Rev. Mod. Phys.* **81**, 109 (2009).
- [2] A. Zolnierski, W. Cetera, D. Jaruga, J. Grzegorek, and G. Sowula, “Graphene and its applications. Study on the development trends in research and on the implementation potential using Big Data and information refining methods,” *J. Nanotechnol. Res.* **4**, 117 (2022).
- [3] N. M. R. Peres, “The transport properties of graphene,” *J. Phys. Cond. Mat.* **21**, 323201 (2009).
- [4] R. W. Keyes, “The electrical properties of black phosphorus,” *Phys. Rev.* **92**, 580 (1953).
- [5] H Asahina and A Morita, “Band structure and optical properties of black phosphorus,” *J. Phys. C: Solid State Phys.* **17** 1839 (1984).
- [6] Xi Ling, H. Wang, S. Huang, F. Xia, and M. S. Dresselhaus, “The renaissance of black phosphorus,” *PNAS* **122**, 4523 (2015).
- [7] Y. Cai, G. Zhang, and Y.-W. Zhang, “Layer-dependent band alignment and work function of few-layer phosphorene,” *Sci. Rep.* **4**, 6677 (2015).
- [8] F. Xia, H. Wang, and Y. Jia, “Rediscovering black phosphorous as an anisotropic layered material for optoelectronics and electronics,” *Nat. Commun.* **5**, 4458 (2014).
- [9] A. Rogalski, M. Kopytko, and P. Martyniuk, “Two-dimensional infrared and terahertz detectors: Outlook and status,” *Appl. Phys. Rev.* **6**, 021316 (2019);
- [10] V. Ryzhii, M. Ryzhii, D. Svintsov, V. Leiman, P. P. Maltsev, D. S. Ponomarev, V. Mitin, M. S. Shur, and T. Otsuji, “Real-space-transfer mechanism of negative differential conductivity in gated graphene-phosphorene hybrid structures: Phenomenological heating model,” *J. Appl. Phys.* **124**, 114501 (2018).
- [11] A. Parappurath, S. Mitra, G. Singh, N. K. Gill, T. Ahmed, T. P. Sai, K. Watanabe, T. Taniguchi, and A. Ghosh, “Interlayer charge transfer and photodetection efficiency of graphene-transition-metal-dichalcogenide heterostructures,” *Phys. Rev. Appl.* **17**, 064062 (2022).
- [12] Z. Guo, H. Zhang, S. Lu, Z. Wang, S. Tang, J. Shao, Z. Sun, H. Xie, H. Wang, X.-F. Yu, and P. K. Chu, “From black phosphorus to phosphorene: Basic solvent exfoliation, evolution of Raman scattering, and applications to ultrafast photonics,” *Adv. Funct. Mater.* **25**, 6996 (2015).
- [13] M. Long, A. Gao, P. Wang, H. Xia, C. Ott, C. Pan, Y. Fu, E. Liu, X. Chen, W. Lu, T. Nilges, J. Xu, X. Wang, W. Hu, and F. Miao, “Room temperature high-detectivity mid-infrared photodetectors based on black arsenic phosphorus,” *Sci. Adv.* **3**, e1700589 (2017).
- [14] V. Ryzhii, T. Otsuji, M. Ryzhii, D. S. Ponomarev, V. E. Karasik, V. G. Leiman, V. Mitin, and M. S. Shur, “Electrical modulation of terahertz radiation using graphene-phosphorene heterostructures,” *Semicond. Sci. Technol.* **33**, 124010 (2018).
- [15] V. Ryzhii, M. Ryzhii V. G. Leiman, V. E. Karasik, V. Mitin, M. S. Shur, and T. Otsuji, “Far-infrared photodetectors based on nanoribbon heterostructures with black-AsP barrier layers,” *Opt. Exp.* **28**, 2480 (2020).
- [16] V. Ryzhii, C. Tang, T. Otsuji, M. Ryzhii, V. Mitin, and M. S. Shur, “Resonant plasmonic detection of terahertz radiation in field-effect transistors with the graphene channel and the black-AsP gate layers,” (submitted),



- arXiv: 2304.11635v1.
- [17] U. Sassi, R. Parret, S. Nanot, M. Bruna S. Borini, D. De Fazio, Z. Zhao, E. Lidorikis, F. H. L. Koppens, A. C. Ferrari, and A. Colli, “Graphene-based mid-infrared room-temperature pyroelectric bolometers with ultrahigh temperature coefficient of resistance,” *Nat. Commun.* **8**, 14311 (2017).
- [18] V. Ryzhii, A. Satou, and T. Otsuji, “Plasma waves in two-dimensional electron-hole system in gated graphene heterostructures,” *J. Appl. Phys.* **101**, 024509 (2007).
- [19] A. N. Grigorenko, M. Polini, and K. S. Novoselov, “Graphene plasmonics,” *Nat. Photonics* **6**, 749 (2012).
- [20] A.V. Muraviev, S. L. Rumyantsev, G. Liu, A. A. Balandin, W. Knap, and M. S. Shur, “Plasmonic and bolometric terahertz detection by graphene field-effect transistor,” *Appl. Phys. Lett.* **103**, 181114 (2013).
- [21] V. Ryzhii, T. Otsuji, M. Ryzhii, V. Mitin, and M. S. Shur, “Resonant plasmonic terahertz detection in vertical graphene-base hot-electron transistors,” *J. Appl. Phys.* **118**, 204501 (2015).
- [22] V. Ryzhii, T. Otsuji, and M. S. Shur, “Graphene based plasma-wave devices for terahertz applications,” *Appl. Phys. Lett.* **116**, 140501 (2019).
- [23] S. Luryi, “Quantum capacitance devices,” *Appl. Phys. Lett.* **52**, 501 (1988).
- [24] S. Dröscher, P. Roulleau, F. Molitor, P. Studerus, C. Stampfer, K. Ensslin, and T. Ihn, “Quantum capacitance and density of states of graphene,” *Appl. Phys. Lett.* **96**, 152104 (2010).
- [25] Z. Tong, A. Pecchia, C. Yam, T. Dumitrică, and T. Frauenheim, “Ultrahigh electron thermal conductivity in T-Graphene, Biphenylene, and Net-Graphene,” *Adv. Energy Mater.* **12**, 2200657 (2022).
- [26] T. Y. Kim, C.-H. Park, and N. Marzari, “The electronic thermal conductivity of graphene,” *Nano Lett.* **16**, 2439-2443 (2016).
- [27] J. H. Strait, H. Wang, S. Shivaraman, V. Shields, M. Spencer, and F. Rana, “Very slow cooling dynamics of photoexcited carriers in graphene observed by optical-pump terahertz-probe spectroscopy,” *Nano Lett.* **11**, 4902 (2011).
- [28] V. Ryzhii, M. Ryzhii, V. Mitin, A. Satou, and T. Otsuji, “Effect of heating and cooling of photogenerated electron-hole plasma in optically pumped graphene on population inversion,” *Jpn. J. Appl. Phys.* **50**, 094001 (2011).
- [29] V. Ryzhii, T. Otsuji, M. Ryzhii, M. Ryzhii, N. Ryabova, S. O. Yurchenko, V. Mitin, and M. S. Shur, “Graphene terahertz uncooled bolometers,” *J. Phys. D: Appl. Phys.* **46**, 065102 (2013).
- [30] V. Ryzhii, A. Satou, T. Otsuji, M. Ryzhii, V. Mitin, and M. S. Shur, “Graphene vertical hot-electron terahertz detectors,” *J. Appl. Phys.* **116**, 114504 (2014).
- [31] V. Ryzhii, T. Otsuji, M. Ryzhii, A. A. Dubinov, V. Ya. Aleshkin, V. E. Karasik, and M. S. Shur, “Negative terahertz conductivity and amplification of surface plasmons in graphene-black phosphorus injection laser heterostructures,” *Phys. Rev. B* **100**, 115436 (2019).
- [32] J. F. Rodriguez-Nieva, M. S. Dresselhaus, and L. S. Levitov, “Thermionic emission and negative dI/dV in photoactive graphene heterostructures,” *Nano Lett.*, **15** 145 (2015).
- [33] V. Ryzhii, T. Otsuji, M. Ryzhii, V. Ya. Aleshkin, A. A. Dubinov, V. Mitin, and M. S. Shur, “Graphene electron transport in van der Waals heterostructures with graphene layers,” *J. Appl. Phys.* **117**, 154504 (2015).
- [34] M. Uda, A. Nakamura, T. Yamamoto, and Y. Fujirnoto, “Work function of polycrystalline Ag, Au, and Al,” *J. Electron Spectros. Relat. Phenomena* **88-91**, 643 (1998).
- [35] B. Liu, M. Köpf, A. N. Abbas, X. Wang, Q. Guo, et al., “Black Arsenic-Phosphorus: Layered anisotropic infrared semiconductors with highly tunable compositions and properties,” *Adv. Mater.* **27**, 4423 (2015).
- [36] F. T. Vasko and V. Ryzhii, “Voltage and temperature dependences of conductivity in gated graphene heterostructures,” *Phys. Rev. B* **76**, 233404 (2007).
- [37] L. A. Falkovsky, “Optical properties of graphene and IV-VI semiconductors,” *Physics-Uspekhi* **51**, 887 (2008).
- [38] V. Ryzhii, D. S. Ponomarev, M. Ryzhii, V. Mitin, M.S. Shur, and T. Otsuji, “Negative and positive terahertz and infrared photoconductivity in uncooled graphene,” *Opt. Mat. Exp.* **9**, 585 (2019).
- [39] A. Rogalski, “Semiconductor detectors and focal plane arrays for far-infrared imaging,” *Opto-Electron. Rev.* **21**, 406 (2013).
- [40] A. S. Mayorov, R. V. Gorbachev, S. V. Morozov, L. Britnell, R. Jalil, L. A. Ponomarenko, P. Blake, K. S. Novoselov, K. Watanabe, T. Taniguchi, and A. K. Geim, “Micrometer-scale ballistic transport in encapsulated graphene at room temperature,” *Nano Lett.*, vol. **11**, 2396 (2011).
- [41] H. Hirai, H. Tsuchia, Y. Kamakura, N. Mori, and M. Ogawa, “Electron mobility calculation for graphene on substrates,” *J. Appl. Phys.* **116**, 083703 (2014).
- [42] Y. Liu, I. Yudhistira, M. Yang, E. Laksono, Y. Z. Luo, J. Chen, J. Lu, Y. P. Feng, S. Adam, and K. P. Loh, “Mediated colossal magnetoresistance in graphene/black phosphorus heterostructures,” *Nano Lett.* **18**, 3377 (2018).
- [43] L. Banszerus, T. Sohler, A. Epping, F. Winkler, F. Libisch, F. Haupt, K. Watanabe, T. Taniguchi, K. Müller-Caspary, N. Marzari, F. Mauri, B. Beschoten, and C. Stampfer, “Extraordinary high room-temperature carrier mobility in graphene-WSe<sub>2</sub> heterostructures,” arXiv:1909.09523v1/
- [44] V. Ryzhii, T. Otsuji, M. Ryzhii, and M. S. Shur, “Double graphene-layer plasma resonances terahertz detector,” *J. Phys. D: Appl. Phys.* **45**, 302001 (2012).
- [45] V. Ryzhii, A. Satou, T. Otsuji, M. Ryzhii, V. Mitin, and M. S. Shur, “Dynamic effects in double graphene-layer structures with inter-layer resonant-tunneling negative conductivity,” *J. Phys. D: Appl. Phys.* **46**, 315107 (2013).
- [46] V. Ryzhii, M. Ryzhii, V. Mitin, M. S. Shur, A. Satou, and T. Otsuji, “Terahertz photomixing using plasma resonances in double-graphene layer structures,” *J. Appl. Phys.* **113**, 174506 (2013).